Direct synthesis of antimicrobial coatings based on tailored bi-elemental nanoparticles

Giulio Benetti,[1,2] Emanuele Cavaliere,[1] Adalberto Canteri,[1] Giulia Landini,[3] Gian Maria Rossolini,[3,4] Lucia Pallecchi,[3] Mirco Chiodi,[5] Margriet J. Van Bael,[2] Naomi Winckelmans,[6] Sara Bals,[6] and Luca Gavioli[1,a]

[1]*Interdisciplinary Laboratories for Advanced Materials Physics (i-LAMP) and Dipartimento di Matematica e Fisica, Università Cattolica del Sacro Cuore, Via Musei 41, 25121 Brescia, Italy*

[2]*Laboratory of Solid State Physics and Magnetism, Department of Physics and Astronomy, KU Leuven, Celestijnenlaan 200D, B-3001 Leuven, Belgium*

[3]*Department of Medical Biotechnologies, University of Siena, Viale Bracci 1, 53100 Siena, Italy*

[4]*Department of Experimental and Clinical Medicine, University of Florence, Via San Damiano, 50134 Florence, Italy*

[5]*Empa, Swiss Federal Laboratories for Materials Science and Technology, Laboratory for Joining Technologies and Corrosion, Überlandstrasse 129, 8600 Dübendorf, Switzerland*

[6]*EMAT University of Antwerp, Groenenborgerlaan 171, B-2020 Antwerp, Belgium*

(Received 10 January 2017; accepted 6 March 2017; published online 20 March 2017)

Ultrathin coatings based on bi-elemental nanoparticles (NPs) are very promising to limit the surface-related spread of bacterial pathogens, particularly in nosocomial environments. However, tailoring the synthesis, composition, adhesion to substrate, and antimicrobial spectrum of the coating is an open challenge. Herein, we report on a radically new nanostructured coating, obtained by a one-step gas-phase deposition technique, and composed of bi-elemental Janus type Ag/Ti NPs. The NPs are characterized by a cluster-in-cluster mixing phase with metallic Ag nano-crystals embedded in amorphous TiO_2 and present a promising antimicrobial activity including also multidrug resistant strains. We demonstrate the flexibility of the method to tune the embedded Ag nano-crystals dimension, the total relative composition of the coating, and the substrate type, opening the possibility of tailoring the dimension, composition, antimicrobial spectrum, and other physical/chemical properties of such multi-elemental systems. This work is expected to significantly spread the range of applications of NPs coatings, not only as an effective tool in the prevention of healthcare-associated infections but also in other technologically relevant fields like sensors or nano-/micro joining. [http://dx.doi.org/10.1063/1.4978772]

The synthesis of tunable and durable microbicidal coatings based on nanoparticles (NPs) is becoming of critical importance[1,2] since indirect transmission of pathogens through contaminated surfaces is a recognized major global health threat, especially in the hospital settings.[3–6] The development of a functional NPs coating implies (1) the capability to tune the composition and the chemical and mechanical[7] properties through a proper combination of its constituting elements in a single NP and (2) the ability to deposit such NPs on a wide variety of substrates, a critical step in achieving an effective microbicidal coating.

So far, the synthesis of NPs composed of two elements (bi-NPs) has stimulated research efforts[8–13] due to their remarkably enhanced catalytic, microbicidal, optical, electronic, and mechanical properties, which goes beyond the mere sum of the effects of the constituent materials. Ag/Fe

[a]Author to whom correspondence should be addressed. Electronic mail: luca.gavioli@unicatt.it

Note: The manuscript was written through contributions of all authors. All authors have given approval to the final version of the manuscript.

NPs allow their removal from a solution after the Ag microbicidal effect has been exploited,[8] while the combination of Au and Pt into bimetallic NPs shows a remarkable microbicidal effect that the single metal NPs (either Au or Pt) do not present.[9] Small quantities of Pd inside Pd-W NPs metal are sufficient to enhance the cluster stability and catalytic properties due to the formation of ultra-active Pd hot-spots.[10] Moreover, Ag can broaden the bactericidal activity of TiO_2-based photocatalyst composite materials and can also act against silver-resistant microorganisms due to their photooxidative mechanism,[14] and various wet synthesis methods have been used resulting in Ag decoration of TiO_2 nanostructures.[15–18]

However, very little is known about the formation and properties of bi-NPs–based coatings.[19] Time-consuming multi-step post-synthesis processes,[19] colloidal stabilizers, cross-linking growth, or substrate functionalization is required to obtain the coating when NPs are synthesized in a wet environment,[19] therefore increasing the degree of complexity of the system. In this respect, the synthesis and the growth of controlled antimicrobial coating with bi-NPs in a single step are an open challenge. A feasible alternative to directly synthesize and deposit controlled nano-structured multi-elemental coatings is based on gas-phase synthesis techniques,[21–23] and in particular Supersonic Cluster Beam Deposition (SCBD).[22,23] Here, the synthesized NPs form a beam that allows the direct deposition of the coating on the substrate. At present, antimicrobial coatings composed of bi-NPs have never been obtained by this approach.

In this work, we present a new family of antimicrobial films composed of bi-elemental Ag–Ti NPs obtained in a single step, with tunable size and relative concentration of the constituents. The NPs are similar to the Janus type NPs,[20] with metallic Ag nano-crystals partly embedded in an amorphous TiO_2 matrix. The nano-structured Ag–Ti coating shows good adhesion to the substrate and exhibits an exceptional bactericidal effect against major Gram-negative nosocomial pathogens, remarkably similar to a pure Ag NPs coating,[24] but with an 85% lower Ag mass content. Thus, this work opens the possibility to produce radically new materials for a variety of applications, engineering the coating properties with a potentially unlimited set of elements: broadening the antimicrobial spectrum for healthcare environments by introducing other microbicidal metals or tailor the coating adhesion by varying the elements relative concentration in the NPs.

The NPs coatings have been obtained by SCBD (see Scheme S1 of the supplementary material), exploiting pulsed plasma ablation of the material to be deposited, and extraction of condensed NPs into a beam directed on the substrate surface. Coatings of three different materials, **AgTi8020** (nominal weight contents 80% Ag and 20% Ti), **AgTi5050** (nominal weight contents 50% Ag and 50% Ti), and **PureAg** (99.99% Ag), were deposited using the same operating conditions independently from the substrate, changing the deposition time to control the film thickness. The antimicrobial features (i.e., reduction of bacterial viability) were investigated against a panel of clinically relevant Gram-negative and Gram-positive nosocomial pathogens, for which contaminated surfaces represent a major vehicle for transmission (Table S5 of the supplementary material).

The SCBD flexibility allows to easily deposit scattered bi-NPs to precisely estimate the height distribution (Figure S1 of the supplementary material) by atomic force microscopy (AFM). For AgTi5050, the bi-NPs median height is 4.3 nm, remarkably higher than the 3.3 nm of AgTi8020 (Figures S1(b) and S1(d) of the supplementary material). Furthermore, the longer tail of the AgTi5050 distribution, extending up to 12 nm, indicates an appreciable increase in the vertical dimension of the bi-NPs with increasing Ti concentration. The NP surface density of the AFM data (Figures S1(b) and S1(d) of the supplementary material) is extrapolated to be 0.02 ± 0.008, much lower than that obtained by aerosol-deposition of TiO2 NP, but in agreement with the prediction of NP deposition in the ballistic regime.[25]

The individual bi-NPs structure has been characterized by high angle annular dark field scanning transmission electron microscope (HAADF-STEM) images (Figure 1), exploiting direct deposition on STEM grids. The NPs are characterized by an intense spot partly surrounded by a lighter gray zone (Figures 1(a) and 1(d)), and the corresponding elemental maps (Figures 1(b) and 1(c)) clearly indicate that the contrast difference is due to Ag (red) and Ti (green) phase-separation. This suggests that SCBD synthesizes aggregates of Ag NPs partly embedded in an amorphous Ti surrounding. An increase of the Ti concentration leads to an increase in the average bi-NP size, related to the formation of aggregates having multiple Ag NPs embedded in the Ti. The obtained NPs are remarkably different from the

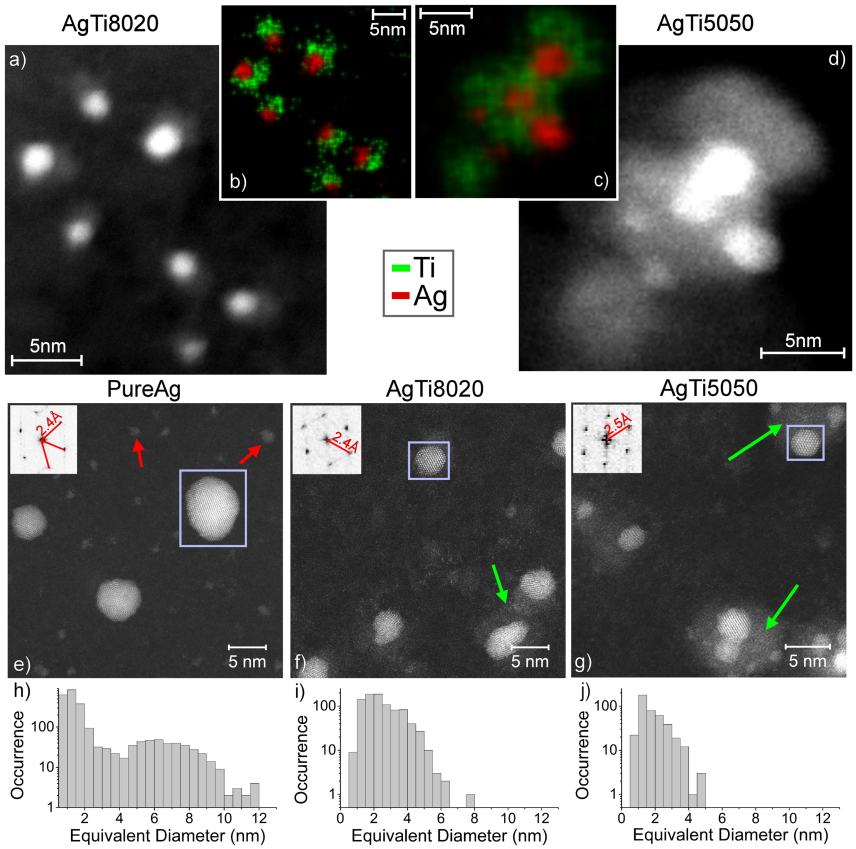

FIG. 1. ((a)–(d)) HAADF images of AgTi8020 and AgTi5050 scattered NPs with the relative elemental map. Short acquisition times are used to limit beam-induced damage (i.e., NPs moving or deforming). ((e)–(g)) High resolution HAADF-STEM images of the NPs and FFT analysis of Ag crystalline structure of the zone in the purple rectangle. Red arrows are indicating small Ag NP, and green arrows are pointing to the Ti part of the NPs. ((h)–(j)) frequency histograms of the Ag crystallites dimension.

simple Ag decoration of TiO_2 nanostructures that have been obtained by sol gel,[14] solvothermal,[15] hydrothermal,[16] and hydrolyzed solution[17] methods.

To obtain statistical information on the bi-NPs size and crystallinity as a function of the Ti concentration, a large number of HR-STEM images were acquired for bi-NPS and for pure Ag NPs (Figures 1(e)–1(g)). The data confirm the Ag and Ti phase separation at the nanoscale. Moreover, the Ag NPs observed in the AgTi8020 and AgTi5050 cases (Figures 1(f) and 1(g)) are mostly polycrystalline, as in the pure Ag phase (Figure 1(e)). Interestingly, the Ti partly surrounding the Ag NP (indicated with green arrows) is completely amorphous instead. The crystallinity of the Ag NPs (either pure or in the Ti) is confirmed by the 2D-fast Fourier transform (FFT) of the purple-squared areas shown in the inserts of Figures 1(e)–1(g). The FFT maxima provide a vector length of 0.24 ± 0.01 nm, compatible with the one of bulk, unstrained Ag{111} spacing (0.236 nm).

Grazing incidence X-ray diffraction (GIXD) obtained on a 100 nm-thick AgTi5050 NP film on glass confirms the presence of Ag nano-crystallites with Ag{111} 0.236 ± 0.002 nm spacing (Figure S2 and Note 3 of the supplementary material), while Ti-related peaks are not found. Hence, the deposited bi-NPs are composed of a mixture of Ag nanocrystals intermixed with amorphous Ti.

The population histograms for Ag NPs diameters are presented in Figures 1(h)–1(j). For pure Ag, the size distribution is characterized by a large number of small NPs (diameter <2 nm (red arrows in Figure 1(e))). Larger NPs with diameters ranging from 4 to 12 nm represent 90% of the total Ag mass (e.g., squared NP in Figure 1(e)). Notably, by increasing the Ti/Ag ratio, the dimension of the Ag nano-crystallites decreases from 2.5 nm, in the case of AgTi8020, to 1.8 nm, in the case of AgTi5050. These results show that SCBD provides an easy and effective way to tailor the Ag NPs size by varying the composition of the sputtered rod. These results are consistent with the AFM data

since STEM images resolve the lateral dimension of Ag nano-crystallites embedded in the Ag–Ti bi-NPs, whereas AFM gives an estimation of the total height of the aggregate including the Ti matrix.

Figure 2 shows Auger electron spectroscopy (AES) and X-ray photoemission spectroscopy (XPS) data taken from three 20 nm-thick NP films deposited on Si(100) having different NPs compositions (see Note 1 and Table S2 in the supplementary material), together with a pure (99.99%) polycrystalline Ag reference.

The data obtained on all NPs coatings and on the pure Ag reference (Figs. 2(a) and 2(b)) do not show any appreciable variation in the intensity or in the energy (both binding, BE or kinetic, KE) for any of the spectral lines, in particular for the oxygen sensitive Ag M_4NN Auger transition,[26–29] indicating that the Ag NPs do not undergo any oxidation. The small lineshape differences found in the AgTi5050 Auger spectrum (shoulder at 348.5 eV and intensity and width of the peak) stem from a Ti Auger line present in the 350–357 eV KE region,[29] becoming relevant with increasing Ti content. The Auger parameter (defined as the Ag $3d_{5/2}$ BE + Ag $M_4N_{4,5}N_{4,5}$ KE) further confirms the purely metallic character of the Ag NPs, see Figure 2(c).[28] Figures 2(d) and 2(e) show the Ti 2p core level and LMV Auger line for AgTi5050 (green dots) and AgTi8020 (blue dots) NPs coatings, respectively. The Ti 2p BE (453.6 eV) and the spin-orbit splitting (5.7 eV) indicate a Ti^{4+} configuration state.[29] Moreover, the energy and the relative area of the two main peaks of the Auger LMV line are compatible with oxidized Ti.[30]

The coating stoichiometry was estimated following the procedure described in Note 4 of the supplementary material (see also the oxygen O1s in Figure 2(f) showing a major contribution from oxygen bonded to Ti at 530.6 eV[31]) and the results are reported in Table TS3: Ag is metallic and Ti is doubly oxidized, hence confirming the morphology of the nanoaggregates as that of Janus Ag–TiO_2 NPs. Moreover, our data clearly indicate that the compositional changes in the pristine rod (i.e., pure Ag, AgTi8020, AgTi5050) correspond to an analogous variation in the produced bi-NPs stoichiometry, proving that SCBD is a powerful tool to tailor the NPs chemical composition simply adjusting the Ag/Ti relative concentration in the initial rod. It is also worth noting that this method has already been used to deposit Np coatings on glass,[24] sapphire,[7] semiconductors,[23] and on PVA electrospun fibers,[32] and can be extended to any metal surface, even textiles and paper, provided they can be inserted into vacuum. Such flexibility can open a wide range of applications of such coatings, from sensors to paper electronics.

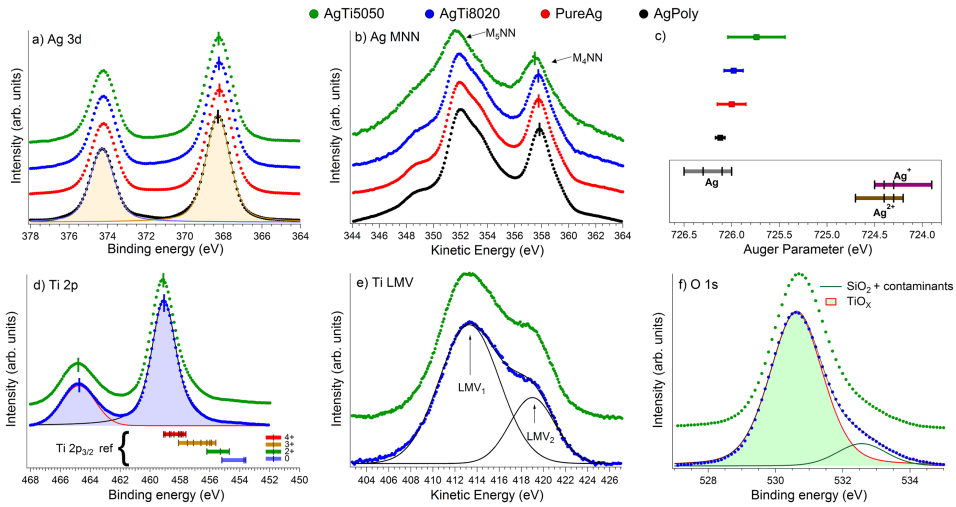

FIG. 2. XPS and Auger data: Pure Ag (red dots), AgTi5050 (green dots), AgTi8020 (blue dots), and polycrystalline Ag (black dots). (a) Ag 3d core level; (b) Ag MNN Auger emission line; (c) experimental Ag Auger parameter compared to the literature. Ag: Refs. 26 and 28; Ag^+: Refs. 26 and 28; Ag^{2+}: Refs. 26 and 28; (d) Ti 2p core levels compared with the literature[31] for different electronic configurations; (e) Ti LMV Auger line: the relative area of Ti LMV peaks indicates the presence of Ti^{4+}; (f) O 1s core level and relative fits. Highlighted area of panels (a), (d), and (f) are used to obtain the relative stoichiometric and mass concentration of the three elements. Fits and quantifications were made for each peak but only the first one is displayed.

The antimicrobial features of the bi-elemental coatings were characterized for the AgTi5050 NPs system, the one with lower Ag amount with respect to a similar coating of ultrapure Ag NPs obtained by SCBD,[24] to reduce the precious metal content in potential applications. The AgTi5050 coatings (thickness of one NPs layer) were found to be extremely effective against all the Gram-negative strains tested (i.e., two reference strains of *Escherichia coli* and *Pseudomonas aeruginosa*, and two multidrug resistant clinical isolates of *P. aeruginosa*, and *Acinetobacter baumannii* (Table S5 of the supplementary material), being able to almost completely sterilize a high bacterial inoculum, $\sim 1 \times 10^7$ colony forming units (CFU), in 3 h (Figure 3(a)).

Shorter exposure times, tested against the multidrug resistant *A. baumannii*, revealed a detectable decrease of viable cells already after 15 min of exposure, with a bactericidal effect (i.e., 3 log reduction of viable cell count) achieved in 90 min (Figure 3(b)). Since environmental surfaces are contaminated with a much lower bacterial inoculum[6] than that used here, the AgTi5050 NP coating, even with a very low Ag content, could be highly effective as an antimicrobial tool in limiting the indirect transmission of Gram-negative pathogens.

An overall lower and slower bactericidal activity was instead observed against the two Gram-positive strains tested (i.e., a reference *Enterococcus faecalis* strain, and a methicillin-resistant *Staphylococcus aureus* clinical isolate exhibiting also non-susceptibility to glycopeptides and daptomycin (Table S5 of the supplementary material)). While a sizable reduction of viable cells was obtained with the *S. aureus* strain after a longer exposition time on AgTi5050 NP films, the *E. faecalis* strain remained substantially unaffected (Figure 3(c)). Overall, the microbicidal activity of AgTi5050 NP films was found to be similar to that of pure Ag NP films synthetized by the same methodology.[24] Indeed, although a direct comparison was not possible due to different substrate types and revised microbiological procedures, a similar reduction in the number of viable bacterial cells was observed with strains tested in both studies, using comparable bacterial inocula for surface contamination. These results encourage further studies to exploit SCBD's ability to produce multi-elemental NPs to include other antimicrobial metals in the NPs coating (possibly broadening the antimicrobial spectrum toward Gram-positive bacteria).

According to Ref. 33 the Ag NP size should have little direct influence on the microbicidal effect, at least on *E. coli*. However, a smaller NP size is influencing the Ag+ ion release due to the higher surface to volume ratio,[34] and hence increasing the microbicidal effect of the AgTi coatings, even more if one consider that part of the Ag NPs might be completely embedded in the TiO_2.

Besides the high antimicrobial performances, the bi-elemental NPs coatings also benefit from the presence of the TiO_2. Due to its ability to act like bridging site at a film/substrate interface, Ti is commonly used to enhance thin films adhesion on various substrates. To verify this effect in our coatings, we performed an empirical comparison between the pure Ag NPs and the AgTi5050 films adhesion on a glass substrate (see Note 5 and Figure S3 in the supplementary material). With respect to the pure Ag NPs, the introduction of Ti remarkably enhances the adhesion without affecting the

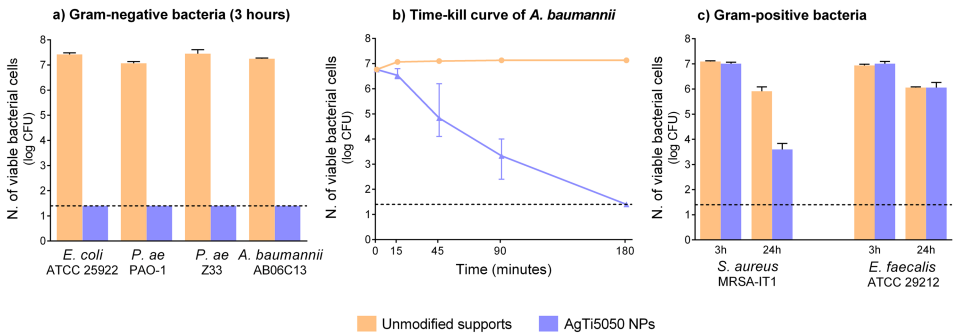

FIG. 3. Antibacterial features of AgTi5050 NP films: (a) antibacterial activity against Gram-negative pathogens (3 h of exposure); (b) time-kill curve of *A. baumannii* AB06C13 (multidrug resistant clinical isolate); (c) antibacterial activity against Gram-positive pathogens (3 and 24 h of exposure). CFU—Colony Forming Unit; P. ae, *Pseudomonas aeruginosa*. Dotted lines indicate the detection limit of viable cell count (1.4 log CFU).

measured antimicrobial activity, saving at the same time more than 85% of the expensive metal (Note 6 of the supplementary material).

In summary, we produced radically new nanostructured coatings using a one-step gas-phase deposition. The coatings are characterized by a cluster-in-cluster mixing phase with small metallic ultra-active microbicidal Ag hot-spots embedded in amorphous TiO_2, stable and strongly bonded to the substrate. Moreover, SCBD allows us to tune the Ag nano-crystals dimension and the total relative composition of the coating. Furthermore, we produced for the first time multi-element NPs by SCBD, opening the possibility of tailoring dimension, composition, antimicrobial spectrum, and other physical/chemical properties of multi-elemental NPs only by varying the native rod's composition. The potential of this technique is also demonstrated by the wide variety of substrates employed (from conductive to insulating substrates, from single crystals to STEM grids, and commercial chromium-coated plastics) and the range of thicknesses obtained, from sub-monolayer (about 1%) up to few hundreds of nm. This work is expected to spread significantly the range of applications of NPs films, not only in the medical field but also in other technologically relevant fields like sensors (where the selectivity to gas absorption is depending on the material employed), nano-/micro joining (where NPs-based pastes are now used as a low-temperature alternatives to standard welding, brazing and soldering processes), or electrocatalysis.

See supplementary material for details of coating preparation, data acquisition, scratch tests, bacterial tests, and the data analysis.

We thank Urs Gfeller for the XRF measurements, Francesco Banfi for valuable discussions on the manuscript and Giulio Viano for his valuable support in the microbiological analysis. The authors acknowledge the financial support of Universita Cattolica del Sacro Cuore through D.2.2 and D.3.1 grants and from the European Union through the 7th Framework Program (FP7) under a contract for an Integrated Infrastructure Initiative (Reference No. 312483 ESTEEM2).

[1] J. A. Lemire, J. J. Harrison, and R. J. Turner, Nat. Rev. Microbiol. **11**, 371 (2013).
[2] E. Faure, C. Falentin-Daudré, T. Svaldo Lanero, C. Vreuls, G. Zocchi, C. Van De Weerdt, J. Martial, C. Jérôme, A. S. Duwez, and C. Detrembleur, Adv. Funct. Mater. **22**, 5271 (2012).
[3] H. Humphreys, Clin. Infect. Dis. **58**, 848 (2014).
[4] D. J. Weber and W. A. Rutala, Am. J. Infect. Control **41**, S31 (2013).
[5] M. M. Quinn and P. K. Henneberger, Am. J. Infect. Control **43**, 424 (2015).
[6] J. A. Otter, S. Yezli, and G. L. French, Infect. Control Hosp. Epidemiol. **32**, 687 (2011).
[7] S. Peli, E. Cavaliere, G. Benetti, M. Gandolfi, M. Chiodi, C. Cancellieri, C. Giannetti, G. Ferrini, L. Gavioli, and F. Banfi, J. Phys. Chem. C **120**, 4673 (2016).
[8] Z. Marková, K. M. Šišková, J. Filip, J. Čuda, M. Kolář, K. Šafářová, I. Medřík, and R. Zbořil, Environ. Sci. Technol. **47**, 5285 (2013).
[9] Y. Zhao, C. Ye, W. Liu, R. Chen, and X. Jiang, Angew. Chem., Int. Ed. Engl. **53**, 8127 (2014).
[10] G. Hu, F. Nitze, E. Gracia-Espino, J. Ma, H. R. Barzegar, T. Sharifi, X. Jia, A. Shchukarev, L. Lu, C. Ma, G. Yang, and T. Wågberg, Nat. Commun. **5**, 5253 (2014).
[11] A. Azam, A. S. Ahmed, M. Oves, M. S. Khan, S. S. Habib, and A. Memic, Int. J. Nanomed. **7**, 6003 (2012).
[12] J. P. Ruparelia, A. K. Chatterjee, S. P. Duttagupta, and S. Mukherji, Acta Biomater. **4**, 707 (2008).
[13] D. Botequim, J. Maia, M. M. F. Lino, L. M. F. Lopes, P. N. Simões, L. M. Ilharco, and L. Ferreira, Langmuir **28**, 7646 (2012).
[14] E. Albert, P. A. Albouy, A. Ayral, P. Basa, G. Csık, N. Nagy, S. Roualdes, V. Rouessac, G. Safran, A. Suhajda, Z. Zolnaif, and Z. Horvolgyi, RSC Adv. **5**, 59070 (2015).
[15] Y. Chen, Y. Deng, Y. Pu, B. Tang, Y. Su, and J. Tang, Mater. Sci. Eng. C **65**, 27 (2016).
[16] F. Liu, H. Liu, X. Li, H. Zhao, D. Zhu, Y. Zheng, and C. Li, Appl. Surf. Sci. **258**, 4667 (2012).
[17] S. A. H. Jalali, A. R. Allafchian, S. S. Banifatemi, and I. Ashrafi Tamai, J. Taiwan Inst. Chem. Eng. **66**, 357 (2016).
[18] H. Cheng, J. Ye, Y. Sun, W. Yuan, J. Tian, R. F. Bogale, P. Tian, and G. Ning, RSC Adv. **5**, 80668 (2015).
[19] K. Yliniemi, M. Vahvaselka, Y. Van Ingelgem, K. Baert, B. P. Wilson, H. Terryn, and K. Kontturi, J. Mater. Chem. **18**, 199 (2008).
[20] D. Wang and Y. Li, Adv. Mater. **23**, 1044 (2011); N. Toshima and T. Yonezawa, New J. Chem. **22**, 1179 (1998).
[21] T. V. Pfeiffer, J. Feng, and A. Schmidt-Ott, Adv. Powder Technol. **25**, 56 (2014).
[22] B. D. Fraters, E. Cavaliere, G. Mul, and L. Gavioli, J. Alloys Compd. **615**, S467 (2014).
[23] M. Chiodi, C. Parks Cheney, P. Vilmercati, E. Cavaliere, N. Mannella, H. H. Weitering, and L. Gavioli, J. Phys. Chem. C **116**, 311 (2012).
[24] E. Cavaliere, S. De Cesari, G. Landini, E. Riccobono, L. Pallecchi, G. M. Rossolini, and L. Gavioli, Nanomed.: Nanotechnol., Biol. Med. **11**, 1417 (2015).
[25] N. Nasiri, T. D. Elmøe, Y. Liu, Q. H. Qin, and A. Tricoli, Nanoscale **7**, 9859 (2015).
[26] G. I. N. Waterhouse, G. A. Bowmaker, and J. B. Metson, Surf. Interface Anal. **33**, 401 (2002).

[27] J. F. Moulder, W. F. Stickle, P. E. Sobol, and K. D. Bomben, *Handbook of X-ray Photoelectron Spectroscopy: A Reference Book of Standard Spectra for Identification and Interpretation of XPS Data* (Physical Electronics, Eden Prairie, MN, USA, 1995), Vol. 72.
[28] A. M. Ferraria, A. P. Carapeto, and A. M. do Rego, Vacuum **86**, 1988 (2012); C. J. Powell, J. Electron Spectrosc. Relat. Phenom. **185**, 1 (2012); S. W. Gaarenstroom and N. Winograd, J. Chem. Phys. **67**, 3500 (1977); V. K. Kaushik, J. Electron Spectrosc. Relat. Phenom. **56**, 273 (1991).
[29] F. Sedona, G. A. Rizzi, S. Agnoli, F. X. Llabrés i Xamena, A. Papageorgiou, D. Ostermann, M. Sambi, P. Finetti, K. Schierbaum, and G. Granozzi, J. Phys. Chem. B **109**, 24411 (2005).
[30] S. Contarini, P. A. W. van der Heide, A. M. Prakash, and L. Kevan, J. Electron Spectrosc. Relat. Phenom. **125**, 25 (2002).
[31] P. R. McCurdy, L. J. Sturgess, S. Kohli, and E. R. Fisher, Appl. Surf. Sci. **243**, 69 (2004).
[32] C. Marega, J. Maculan, G. A. Rizzi, R. Saini, E. Cavaliere, L. Gavioli, M. Cattelan, G. Giallongo, A. Marigo, and G. Granozzi, Nanotechnology **26**, 075501 (2015).
[33] Z.-M. Xiu, Q.-bo Zhang, H. L. Puppala, V. L. Colvin, and P. J. J. Alvarez, Nano Lett. **12**, 4271 (2012).
[34] B. Le Ouay and F. Stellacci, Nano Today **10**, 339 (2015).